Effects of reducing the reactor diameter on thedense gas–solid fluidization of very heavyparticles: 3D numerical simulations

Renaud Ansart, Florence Vanni, Brigitte Caussat, Carine Ablitzer, Méryl Brothier

Effects of reducing the reactor diameter on the dense gas–solid fluidization of very heavy particles: 3D numerical simulations

Renaud Ansart[a,*], *Florence Vanni*[a,b], *Brigitte Caussat*[a], *Carine Ablitzer*[b], *Méryl Brothier*[c]

[a] *Laboratoire de Génie Chimique, Université de Toulouse, CNRS, INPT, UPS, Toulouse, France*
[b] *CEA Cadarache DEN, DEC/SFER, Laboratoire des Combustibles Uranium, F-13108 Saint-Paul Lez Durance, France*
[c] *CEA Marcoule DEN, DTEC/SECA Service d'Etude des Combustibles et matériaux à base d'Actinides, F-30207 Bagnols sur Cèze, France*

In this study, 3D numerical simulations using an Eulerian n-fluid approach of a gas–solid fluidized bed composed of very dense particles of tungsten (19,300 kg m^{-3}) were carried out to examine the behavior of this suspension, especially the effects of the reduction of the fluidization column diameter on the fluidization quality. Tungsten was selected as a surrogate material of U(Mo) (Uranium molybdene) which is of interest for new nuclear fuels with limited enrichment. Comparisons between experiments and computations for the axial pressure profile of a 5 cm diameter column demonstrate the capability of the mathematical models of the NEPTUNE_CFD code to simulate the fluidization of this powder located outside the classification of Geldart. The numerical results show that the mobility into the bed of these very dense particles is very low. The reduction of the fluidization column diameter from 5 cm to 2 cm does not have significant effect on the local solid circulation but strongly decreases the axial and radial mixing of the particles due to wall-particles friction effects. These results confirm and allow to better understand the wall effects experimentally evidenced.

Keywords:
Fluidization
CFD simulation
Very dense particles suspension
Euler–Euler modeling
Micro fluidized bed

1. Introduction

Gas–solid fluidized beds (FB) are widely used in industrial applications such as drying, coal combustion (Basu, 1999) and gasification (Hofbauer et al., 2002), oil refining and nuclear application (Kunii and Levenspiel, 1991). This is due to the fact that FB reactors have excellent heat and mass transfer capabilities, high throughput rates, and can operate continuously, thus reducing operating costs (Ydstie and Du, 2011; Liu and Xiao, 2014).

In the nuclear field, new fuels, with limited enrichment in ^{235}U, are under development for research reactors. U(Mo) (Uranium molybdene) fuel powders dispersed in an aluminum matrix are among the most promising materials. But the coating of U(Mo) by a barrier material is necessary to limit interfacial interactions between the fuel and its matrix under irradiation (Mazaudier et al., 2008). Silicon seems to be a good candidate (Zweifel et al., 2013). Among other technics, the Fluidized Bed Chemical Vapor Deposition process (FB-CVD) is under study to deposit uniform silicon layers on U(Mo) particles (Vanni et al., 2015a). FB-CVD is an efficient technology to uniformly coat powders by a great variety of materials (Vahlas et al., 2006). There is an interest in being able to treat weights of U(Mo) as low as possible by the FB-CVD process. It is to

* *Corresponding author.*
E-mail address: renaud.ansart@ensiacet.fr (R. Ansart).
http://dx.doi.org/10.1016/j.cherd.2016.11.008

Nomenclature

Roman symbols

Ar	Archimede number (–)
d_p	particle diameter (m)
e_c	particle–particle normal restitution coefficient (–)
g	gravitational constant ($m\,s^{-2}$)
m_p	particle mass ($kg\,m^{-3}$)
P	mean gas pressure ($N\,m^{-2}$)
q_p^2	random kinetic energy ($m^2\,s^{-2}$)
$U_{k,i}$	mean velocity of phase k ($m\,s^{-1}$)
U_{mf}	minimum fluidization velocity ($m\,s^{-1}$)
$u'_{k,i}$	fluctuating velocity of phase k ($m\,s^{-1}$)
V_f	superficial gas velocity ($m\,s^{-1}$)

Greek symbols

α_k	volume fraction of phase k (–)
μ_g	gas viscosity ($kg\,m^{-1}\,s^{-1}$)
ρ_k	density of phase k ($kg\,m^{-3}$)
Θ_p	granular temperature ($kg\,m^{-2}\,s^{-2}$)

Subscripts

g	gas
p	particle

be noted that for preliminary experiments a tungsten powder (19,300 $kg\,m^{-3}$, 75 μm of median diameter) whose properties are very close to those of U(Mo) (17,500 $kg\,m^{-3}$, 50 μm median diameter) has been used as a surrogate powder. Both powders are of very high density. The maximum dimensionless density is 10,000 in the Geldart's classification, but the dimensionless density of the tungsten particles clearly exceeds the upper limit (Fig. 1). First experiments have demonstrated that the FB-CVD technology can uniformly coat 1,500 g of tungsten powder with silicon in a reactor of 3.8 cm in diameter. Other experiments have shown that this weight cannot be decreased in the reactor of 3.8 cm because the target deposition temperature (650 °C) cannot be reached since heat exchange between the reactor walls and the bed of particles becomes too low (Vanni et al., 2015a).

An experimental study has been conducted in glass and steel columns to specifically analyze the impact of decreasing

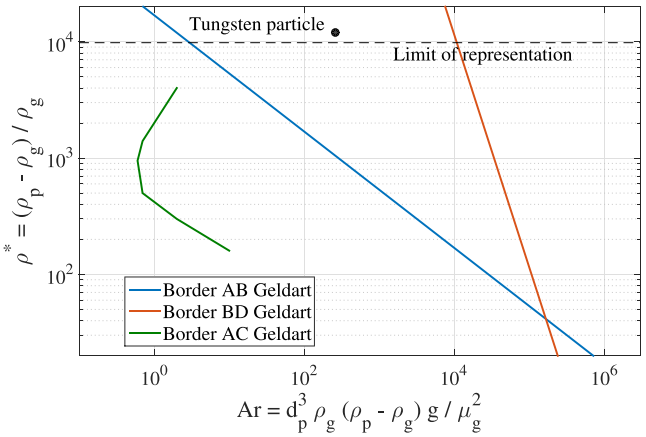

Fig. 1 – Representation of the tungsten particles with a diameter of 75 μm in Geldart's classification modified by Yang (2007).

the reactor diameter from 5 to 2 cm on the fluidization hydrodynamics of the tungsten powder (Vanni et al., 2015b). It was found that uniform silicon deposition could only be achieved if the fluidized bed hydrodynamics was of good quality, i.e. if it involves high thermal and mass transfer rates between the gas and the solid phases. This experimental study has shown that wall effects decreasing the quality of bed hydrodynamics appear in the reactor of 2 cm for 100 g and 180 g of powder. This was evidenced by an increase of the hysteretic behavior of the pressure drop curves, an increase of the minimum fluidization velocity and a decrease of the bed voidage. This was especially evident in a glass column where the electrostatic effects cannot be neglected (Vanni et al., 2015b).

The aim of the present study is to complement the experimental work by using 3D numerical simulations to analyze more precisely the influence of a decrease of the reactor diameter on some key local parameters of the fluidized bed hydrodynamics. The results are expected to be helpful in the FB-CVD process design and in the choice of its optimal gas flow parameters.

Very few studies are available in the literature about the numerical simulation of fluidized beds involving such dense particles. For UO_2 particles of 2 mm in diameter, Liu et al. (2015a) studied the impact of particle density up to 10,800 $kg\,m^{-3}$ on the fluidization behavior of particles in spouting bed using 2D CFD-DEM coupling. The particle cycle time, spout behavior, dominant spout frequency and gas–solid contact efficiency was discussed and a flow pattern map under different densities and different gas velocities was obtained. Pannala et al. (2007) also studied conical spouted bed with heavy particles (up to 6,050 $kg\,m^{-3}$ zirconia particles for nuclear fuel coaters) by 2-D Eulerian–Eulerian numerical simulations.

Miniaturization of chemical reactors, which is one of the most popular research areas in chemical engineering, has led to the concept of micro-fluidized bed reactors (Wang et al., 2011). Wang et al. (2011) have shown by CFD simulations that for Geldart A particles, the onset of turbulent fluidization is advanced significantly in micro fluidized beds. Zivkovic and Biggs (2015) pointed out the importance of wall surface forces relative to volumetric forces, such as gravity, on micro-scale fluidized beds (the cross-sectional dimensions of the microchannels were $400 \times 175\,\mu m^2$). Liu et al. (2015b) performed several 2D Eulerian–Eulerian numerical simulations for a gas–solid micro-fluidized bed (channel width 3 mm) for Geldart A particles (53 μm and 1,400 $kg\,m^{-3}$) and compared the predicted minimum bubbling velocity and bed voidage to experimental measurements. They used very fine meshes (of approximately one particle diameter). Using the Gidaspow drag model, their simulations have shown that the predicted minimum bubbling velocities were significantly lower than their experimental data (Liu et al., 2015b). Wang and Fan (2011) have established a flow regime map from experimental results obtained in column diameters starting from 0.7 mm to 5 mm in size for FCC particles. Their results revealed an increase in the minimum fluidization and bubbling velocities compared to those in large-scale fluidized beds. To the best of our knowledge, no numerical work has been reported concerning reduced diameter fluidized beds of heavy particles, which are studied in the present article.

The experimental fluidization set-up will be first presented before detailing the numerical model and presenting and discussing the results of the simulation.

Table 1 – Particle properties and particle size distribution characteristics of the tungsten particles obtained with a Malvern Master Sizer Sirocco 2000 in dry mode.

Mean diameter	Value (μm)
$d_{3/2}$	70
d_{10}	50
d_{50}	75
d_{90}	105
Density	**Value ($kg\,m^{-3}$)**
Particle	19,300
Bulk	9,600
U_{mf} (Thonglimp et al., 1984)	3.2 $cm\,s^{-1}$

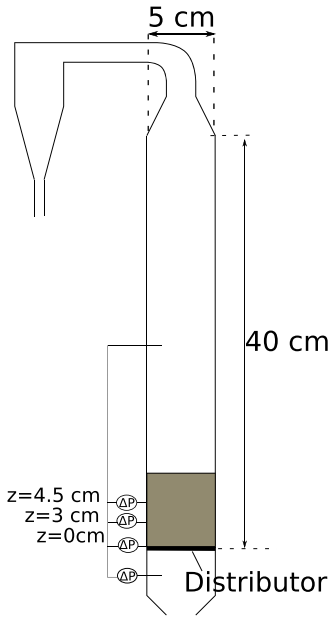

Fig. 2 – Schematic of the experimental setup.

2. Experimental set up

The experimental set up is composed of three steel columns of 1 m height and 5, 3 and 2 cm of inner diameter (Vanni et al., 2015b). All are equipped with a similar Inox porous plate distributor (Poral^{TM} 40). The tungsten powder used (CERAC, Inc. T-1220) is supplied by Neyco. Its grain density is claimed to be 19,300 $kg\,m^{-3}$. The Particle Size Distribution characteristics of the powder are summarized in Table 1 with its bulk density. The experiments were conducted at ambient temperature using argon as the fluidizing gas. Its flow rate was controlled by a mass flow controller (Aera FC-7710 C0, 0-20 slm). A differential fast response pressure sensor (GE Druck LPX 5380), with taps under the distributor and on top of the column, was used to measure the total pressure drop across the bed and determine the minimum fluidization velocity. Three other pressure sensors were set on the 5 cm column at 0 cm, 3 cm and 4.5 cm above the distributor to measure the axial pressure profile (Fig. 2). The sampling rate for pressure measurement is 2 Hz and the time-averages are realized during 2 min.

3. Numerical simulation description: Euler n-fluid approach

Three-dimensional numerical simulations are carried out using the code NEPTUNE_CFD. This Eulerian n-fluid unstructured parallelized multiphase flow software has been developed in the framework of the NEPTUNE project financially supported by CEA (Commissariat à l'Energie Atomique et aux énergies alternatives), EDF (Electricite de France), IRSN (Institut de Radioprotection et de Sureté Nucléaire), and AREVA-NP (Méchitoua et al., 2003). The modeling approach for poly-dispersed fluid-particle flows is implemented by the Institut de Mécanique des Fluides de Toulouse (IMFT) in the NEPTUNE_CFD V1.08 version. The numerical solver has been developed for High Performance Computing (Neau et al., 2010, 2013).

3.1. *Mathematical models*

The Eulerian n-fluid approach used is a hybrid method (Morioka and Nakajima, 1987) in which the transport equations are derived by phase ensemble averaging for the continuous phase and by use of the kinetic theory of granular flows supplemented by fluid effects for the dispersed phase. The momentum transfer between gas and particle phases is modeled using the drag law of Wen and Yu (Wen and Yu, 1965), limited by the Ergun (Ergun, 1952) equation for dense flows (Gobin et al., 2003; Fede et al., 2016). The collisional particle stress tensor is derived in the frame of the kinetic theory of granular media (Boëlle et al., 1995). In the present study the gas flow equations are treated as laminar because the gas Reynolds stress tensor in the momentum equation is negligible compared to the drag term. For the solid phase, a transport equation for the particle fluctuant kinetic energy, q_p^2, is solved. According to the large inertia of the particles and to the low inelasticity of particles ($e_c = 0.9$), the spatial correlation between neighboring particle fluctuant velocities will remain negligible (Fox, 2014; Fevrier et al., 2005; Simonin et al., 2002). The particle fluctuating motion may be assumed spatially uncorrelated obeying the so called molecular chaos assumption so that the product of the particle mass and particle fluctuant kinetic energy $m_p q_p^2$ can be identified to the granular temperature Θ_p defined in spatial granular flow theories (Lun and Savage, 1986).

The gas–particle turbulent correlation is negligible. The effects of the particle–particle contact force in the very dense zone of the flow are taken into account in the particle stress tensor by the additional frictional stress tensor (Srivastava and Sundaresan, 2003). All the equations of the Euler–Euler approach are detailed in Fotovat et al. (2015).

3.2. *Numerical parameters*

3.2.1. *Geometry*

The reference fluidized bed is a column of 5 cm in diameter and 40 cm in height with a conical portion at its top end. The influence of the column diameter reduction is analyzed by comparison with columns of 3 and 2 cm in diameter and of similar height.

3.2.2. *Mesh*

The 3D reference mesh (Fig. 3) is composed of 277,635 hexahedra, based on O-grid technique with 50 cells on the column diameter and approximately $\Delta_x = \Delta_y \approx 1$ mm and $\Delta_z = 1.9$ mm. It is noteworthy that a finer mesh, refined of 1.5 in each space direction, has been tested but no mesh refinement effect was observed on the bed height and on the time-averaged radial profiles of solid volume fraction, solid velocity and solid time variance velocity.

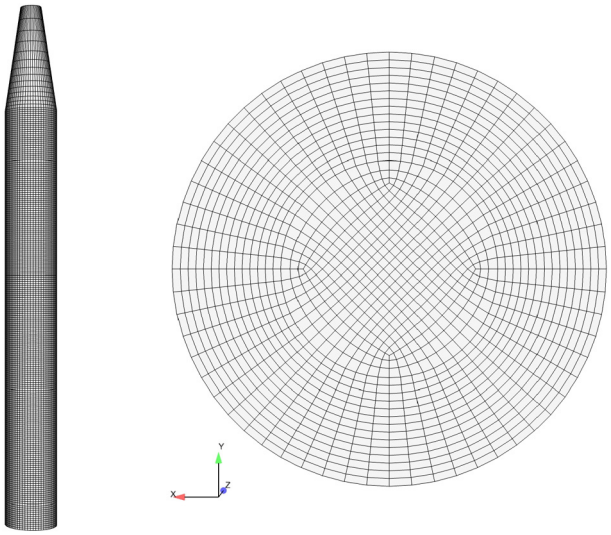

Fig. 3 – 3D mesh for the numerical simulation with 277,635 cells.

Table 2 – Phases' properties used for the simulation.

Parameters	Value
Gas density (Argon)	1.6 kg m^{-3}
Gas viscosity	2.23 × 10^{-5} Pa s
Particle diameter	70 μm
Particle density	19, 300 kg m^{-3}

The meshes for the 3 and 2 cm column diameter have exactly the same number of cells and were obtained by applying homothetic transformation.

3.2.3. *Phase properties*

The flow is composed of two phases: gas (argon) and tungsten particles. The phases' properties are summarized in Table 2. The particles are assumed to be spherical with a monodisperse diameter equal to the Sauter diameter. The authors have tested simulations with the median diameter but discrepancy with experimental results were observed especially for the prediction of the minimum fluidization velocity.

3.2.4. *Boundary conditions*

At the bottom (z = 0), the fluidization grid is an inlet for the gas with an imposed uniform superficial velocity (V_f) corresponding to the fluidization velocity and a wall for the particles. At the top of the fluidized bed, a free outlet for both gas and particles is defined. The wall-type boundary condition is no-slip for the gas and for the particles (Fede et al., 2016).

3.2.5. *Initial conditions*

The solid masses used in each column are detailed in Table 3. They correspond to a ratio between the fixed bed height and the column diameter H_0/D close to 3.

3.2.6. *Simulation progress*

The numerical simulations have been performed on parallel computers with 20 cores. A numerical simulation is divided into two steps: a transitory step of 10 s corresponding to the establishment of the hydrodynamics of the fluidized bed and an established regime during which the statistics are computed for 100 s. The numerical radial profiles presented in this study are from the *O–x* direction but they are symmetrical with the profiles of the *O–y* direction. The authors have checked that all time-averaged bed values are axisymmetric.

Table 3 – Solid masses.

Column	5 cm	3 cm	2 cm
Mass of solid (g)	2,827	741	181

Table 4 – Experimental and predicted minimum fluidization velocities.

U_{mf} (cm s^{-1})	D = 5 cm	D = 3 cm	D = 2 cm
Exp. glass column	2.92	3.82	4.11
Exp. steel column	3.14	3.02	3.19
Simulation	3.41	3.50	3.82

4. Results and discussion

As shown in Fig. 4, Vanni et al. (2015b) have observed wall effects for a 2 cm glass column, consisting in an increase of the hysteretic behavior between increasing and decreasing pressure drop curves and of the minimum fluidization velocity in the glass column. This observation is less marked in the steel column due to the reduction of electrostatic forces.

Defluidization curves in Fig. 5 present a comparison between numerical results and experimental measurements carried out of the total bed pressure drop at decreasing gas velocity in the steel column Vanni et al. (2015b). The horizontal dashed lines correspond to the theoretical bed pressure drop (equal to the bed weight per column surface area). A relative good agreement can be observed. However, the numerical results slightly underestimate the pressure in the fixed bed part. This leads to an overestimation of the minimum fluidization velocity as detailed in Table 4. This slight overestimation of the minimum fluidization velocity can be attributed to the non regular shape of particles (Fig. 6). It is noteworthy that the numerical results predict an increase of the minimum fluidization velocity for the column of 2 cm as the experimental ones, confirming the existence of wall effects. The Thonglimp et al. (1984) correlation was used to calculate U_{mf}. The value of 3.2 cm s^{-1} was found logically close to the experimental U_{mf} value in the steel 5 cm column where the electrostatic and wall effects are minimum.

For the following simulations, the gas fluidization velocity has been fixed at 12 cm s^{-1}. The fluidization ratio is then close to 3 for the columns of 5 and 3 cm and to 2.8 for the column of 2 cm. The minimum fluidization velocities used to calculate the fluidization ratio are the experimental ones. They are extracted from Fig. 5 using the Davidson and Harrison method (Davidson et al., 1963).

The predicted time-averaged gas pressure at the wall as a function of height for the three steel columns is presented in Fig. 7. The numerical data were extracted from the cells directly at the wall to plot these curves. For all cases, the gas pressure drop is linear inside the bed with almost the same slope. The pressure gradient is then constant and is not a function of the column diameter. Moreover, the experimental measurements for the column of 5 cm show a very good agreement with the numerical values.

Table 5 shows the time-averaged pressure gradient predicted at the wall. The values of the pressure gradient inside the bed for the different columns are almost the same as previously observed. Using this pressure gradient at the wall, the void fraction of the overall fluidized bed has been estimated

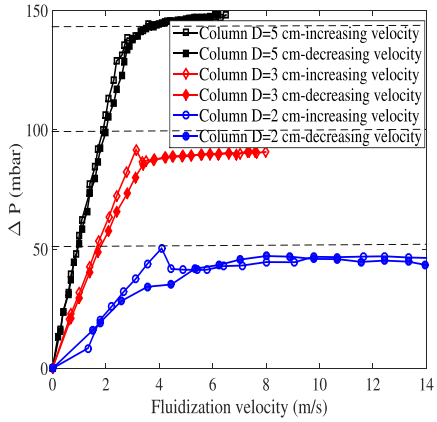

(a) Glass columns.

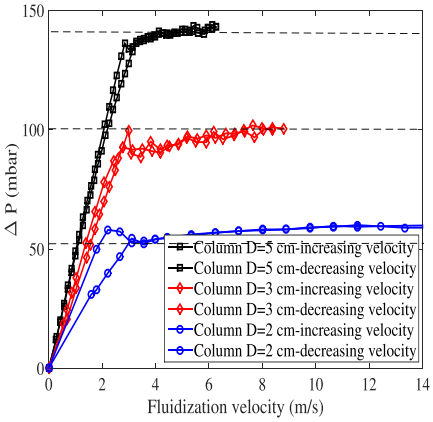

(b) Steel columns.

Fig. 4 – Experimental bed pressure drop curves in the glass and steel columns for $H_0/D = 3$.

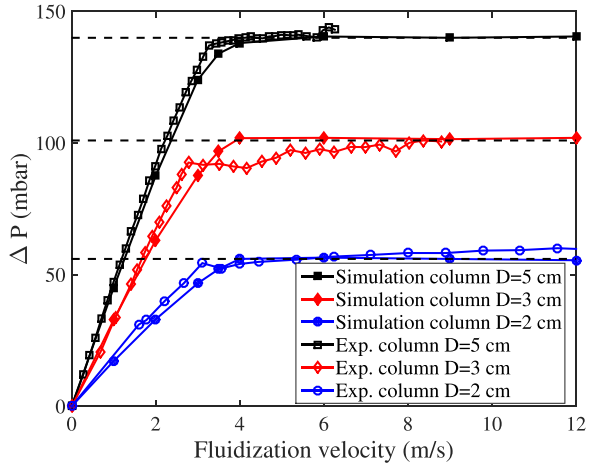

Fig. 5 – Comparison between experimental measurements for steel column and numerical results of the bed pressure drop curves obtained at decreasing gas flow rate.

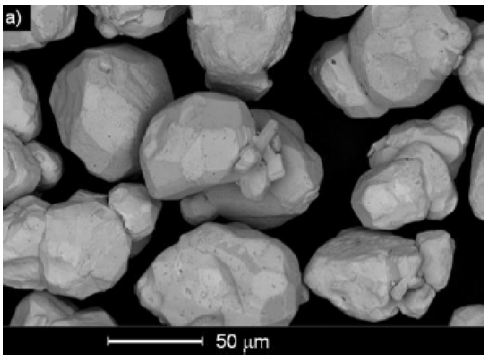

Fig. 6 – SEM view of tungsten particles.

Table 5 – Time-averaged gas pressure drop, bed height and solid volume fraction, $V_f = 12\,\mathrm{cm\,s^{-1}}$.

Column	5 cm	3 cm	2 cm
$\Delta P/L$ (mbar m^{-1})	1,006	1,012	1,017
Bed height (cm)	13.79	10.05	5.55
$\bar{\alpha_g}$	0.468	0.465	0.462
$\langle\alpha_g\rangle$	0.497	0.512	0.517
error($\bar{\alpha_g}$, $\langle\alpha_g\rangle$)	6.1%	10.1%	11.9%

by neglecting the friction forces of the particles at the wall and assuming an equilibrium between the buoyancy and the drag forces:

$$\bar{\alpha_g} = 1 - \frac{1}{(\rho_p - \rho_g)g}\frac{\Delta P}{L} \tag{1}$$

This estimation of the bed void fraction can be compared to the mean volume fraction obtained by integrating the local void fraction over the entire cells of the computational domain:

$$\langle\alpha_g\rangle = \int\int\int_{\mathcal{V}_{bed}} \alpha_g \, d\mathcal{V} \tag{2}$$

This comparison (last line, Table 5) shows that the relative error increases with the reduction of column diameter. Hence, for the conditions tested, the friction forces at the wall can not be neglected anymore for a 2 cm column of fluidization. The smaller the column diameter is, the higher are the wall-particle friction forces. When the column diameter decreases, the ratio between the wall surface and the particles volume increases which generates a lifting effect of the bed. Thus, the reduction of the column diameter increases the void fraction causing the bed expansion. No experimental measurements

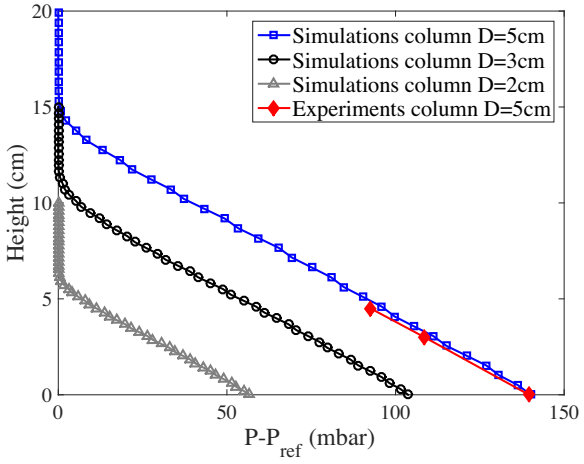

Fig. 7 – Time-averaged axial profiles of gas pressure at the wall from numerical simulations and experimental measurements (P_{ref} is a value above the dense fluidized bed), $V_f = 12\,\mathrm{cm\,s^{-1}}$.

Table 6 – Phases properties used for the simulation of sand particle.

Parameters	Value
Gas density (Argon)	1.6 kg m^{-3}
Gas viscosity	2.23 × 10^{-5} Pa s
Sand particle diameter	206 μm
Sand particle density	2,600 kg m^{-3}
U_{mf} (Thonglimp et al., 1984)	3.2 cm s^{-1}

have been performed in the steel column to be compared with these predicted values.

Some time-averaged radial profiles have been calculated at 2/3 of the bed height. The bed height has been determined (Table 5) from the changing slope of the axial profiles of the time-averaged gas pressure (Fig. 7). Consequently, the profiles were extracted on one cell at the position of z = 9.1 cm, 6.6 cm and 3.6 cm respectively for the columns of 5 cm, 3 cm and 2 cm.

Fig. 8(a) shows the time-averaged radial profile of the solids volume fraction. Numerical predictions present a minimum at the center of the tube and a maximum near the wall. This trend is the same as that normally observed for classical Geldart group B particles. However, by performing specific simulations with sand particles (Table 6) of similar minimum fluidization velocity, we have verified that the fluidization of tungsten powder shows high solid volume fraction in comparison to results obtained for more conventional sand particles. Thus, the expansion of this powder is lower than for sand particles. Moreover, it is noteworthy that the reduction of column diameter induces a reduction of the extrema of the time-averaged radial profile of the solids volume fraction and so an increase of the mean bed void fraction. This effect confirms the previous observations on the increase of the void fraction.

Fig. 8(b) and (c) shows respectively the time-averaged vertical component of solid phase velocity and the associated solid mass flux. The radial profiles are similar with a positive maximum value at the center and a negative minimum one close to the wall due to bubble rise in the center of the tube. Because the size and then the velocity of the bubbles are limited by the reduction of the column diameter, the maximum of the particle velocity decreases.

The particles rise at the center of the column is observed in Fig. 9 which shows the solid velocity vectors for the three columns. An upward solid flow in the center of the tube and a downward more concentrated solid flow near the wall are clearly observed with the formation of two 2D loops (resulting in torus in 3D cylindrical geometry) at the bottom and at the top of the fluidized bed. As can be noticed, the reduction of the column diameter does not influence the local behavior of the particles in the fluidized bed. Such a conical circulation pattern has already been observed in dense fluidized bed (Fotovat et al., 2015; Werther and Molerus, 1973).

Fig. 8(d) presents the time-averaged granular temperature of particles, which represents the frequency of particle–particle collisions. For the three columns, it presents a maximum at the center of the tube and a minimum near the wall. It is noteworthy that the granular temperature of tungsten particles is more than fifteen times lower than for the sand particles for a fluidization ratio of 4. This means

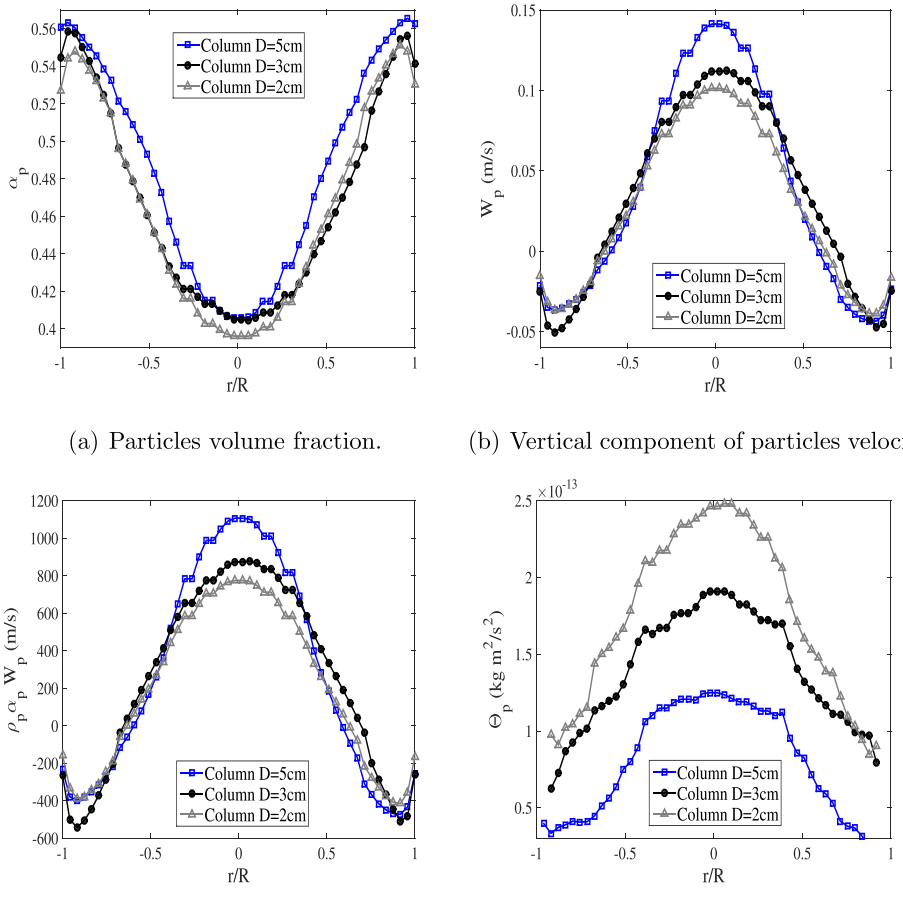

(a) Particles volume fraction.

(b) Vertical component of particles velocity.

(c) Vertical solid mass flux.

(d) Granular temperature.

Fig. 8 – Effect of column diameter on the time-averaged flow variables radial profiles at z = 2/3× bed height, V_f = 12 cm s^{-1}.

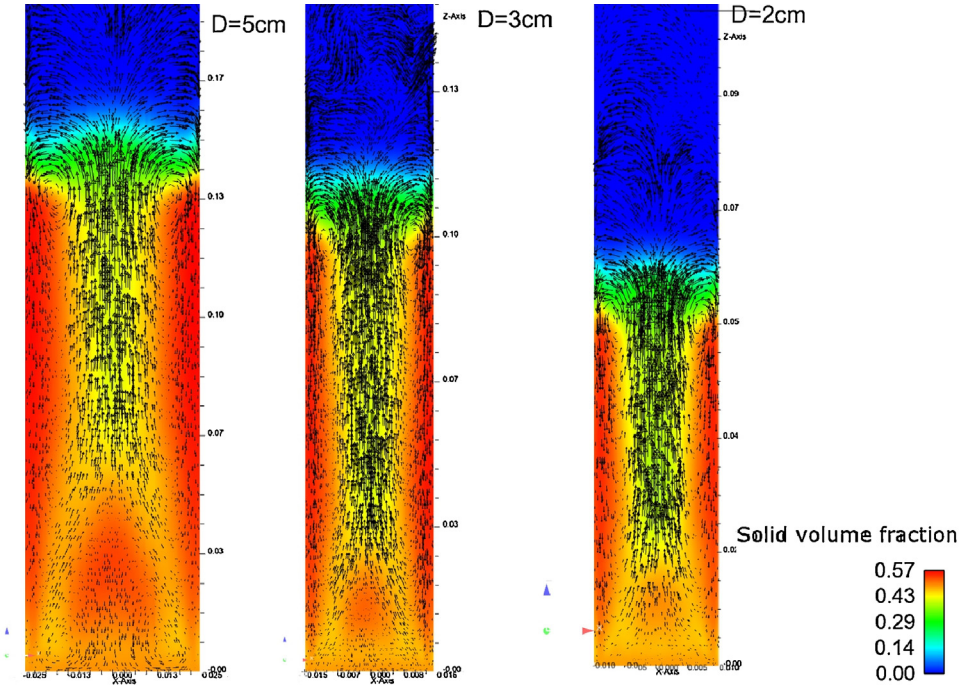

Fig. 9 – Cross sectional view at the center of the column of the time-averaged volume fractions and of the streamlines of the tungsten particles velocity, $V_f = 12\,\mathrm{cm\,s^{-1}}$.

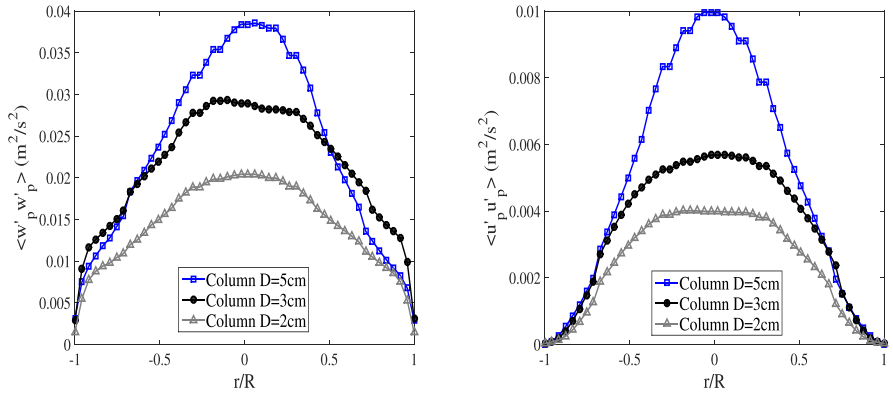

(a) Time-variance of the vertical component of solid phase velocity.

(b) Time-variance of the horizontal component of solid phase velocity.

Fig. 10 – Effect of column diameter on the time-averaged flow variables radial profiles at $z = 2/3\times$ bed height, $V_f = 12\,\mathrm{cm\,s^{-1}}$.

that the high density of the tungsten particles tends to drastically reduce the frequency of particle–particle collisions. The granular temperature increases with the reduction of the column diameter due to an increase of the solid shear stress at the wall. The mean granular temperature for the column of 2 cm is twice higher than for the column of 5 cm. So, the reduction of the column diameter increases the frequency of particle–particle collisions but this remains notably lower than for conventional powders.

Fig. 10(a) and (b) presents the time-variance of the vertical and horizontal solid phase velocities. The time-variance of the vertical component of solid velocity is maximum at the center and minimum near the wall and the standard deviation is approximatively of the same order as the time-averaged velocity. The time-variance of vertical velocity of tungsten particles is of the same order as that of sand particles but the time-variance of horizontal velocity is three times lower. The time-variance of the vertical and the horizontal components of solid velocities decreases with the reduction of the column diameter due to the confinement effect. This means that the solid mixing in the fluidized bed decreases confirming the wall effects experimentally observed. This result can also explain that the heat transfer rates between the particles and the reactor walls decrease with the column diameter, as observed experimentally (Vanni et al., 2015b).

First CVD experiments have shown that the conversion rate of silane is lower than for conventional powders. This can be explained by the simulation results, indicating a lower particle mobility and a lower particle mixing for these very dense tungsten particles (Vanni et al., 2015a).

5. Conclusion

3D numerical simulations, using an Eulerian 2-fluid method, were performed in this work to analyze the hydrodynamics of very heavy particles of tungsten, located outside the classical classification of Geldart, in a dense gas–solid fluidized bed.

The aim was to study the influence of the reduction of column diameter.

The simulations are successful in reproducing the experimental measurements of axial gas pressure drop and the increase of minimum fluidization velocity by decreasing the column diameter from 5 cm to 2 cm. The numerical results pointed out that the reduction of column diameter increases the void fraction in the dense fluidized bed due to wall-particle friction effects. From 5 cm to 2 cm of column diameter, the particles have a conventional local circulation with the solids rising in an annular zone of increased bubble development in the column center and then descending near the wall.

However, the very high density of tungsten particles tends to drastically reduce their mobility inside the bed. Moreover, the reduction of column diameter decreases the solid mixing, confirming the wall effects experimentally observed.

As the measurements have shown that the tungsten particles can easily become electrostatically charged, future numerical simulations will take this fact into account, in order to improve the predictive capability of the model. Finally, future experimental research opportunities would be to carry out experiments on the local behavior of dense gas–tungsten particle suspension. It would be interesting to access to the bubbles size and velocity using appropriate probes and according to the particles trajectory from Radioactive Particle Tracking (RPT) or to Positron Emission Particle Tracking (PEPT) measurements to determine the particle velocity.

Acknowledgements

This work was granted access to the HPC resources of CALMIP under the allocation P11032 and CINES under the allocation gct6938 made by GENCI. The authors acknowledge helpful comments provided by Professor Olivier Simonin.

References

Basu, P., 1999. Combustion of coal in circulating fluidized-bed boilers: a review. Chem. Eng. Sci. 54 (22), 5547–5557.

Boëlle, A., Balzer, G., Simonin, O., 1995. Second-order prediction of the prediction of the particle-phase stress tensor of inelastic spheres in simple shear dense suspensions. Gas–Particle Flows, ASME FED, vol. 28., pp. 9–18.

Davidson, J., Harrison, D., Jackson, R., 1963. Fluidized Particles. Cambridge University Press, 155 pp. 35s, 1964.

Ergun, S., 1952. Fluid flow through packed columns. Chem. Eng. Prog. 48, 89–94.

Fede, P., Simonin, O., Ingram, A., 2016. 3D numerical simulation of a lab-scale pressurized dense fluidized bed focussing on the effect of the particle–particle restitution coefficient and particle-wall boundary conditions. Chem. Eng. Sci. 142, 215–235.

Fevrier, P., Simonin, O., Squires, K.D., 2005. Partitioning of particle velocities in gas–solid turbulent flows into a continuous field and a spatially uncorrelated random distribution: theoretical formalism and numerical study. J. Fluid Mech. 533, 1–46.

Fotovat, F., Ansart, R., Hemati, M., Simonin, O., Chaouki, J., 2015. Sand-assisted fluidization of large cylindrical and spherical biomass particles: experiments and simulation. Chem. Eng. Sci. 126, 543–559.

Fox, R.O., 2014. On multiphase turbulence models for collisional fluid-particle flows. J. Fluid Mech. 742, 368–424.

Gobin, A., Neau, H., Simonin, O., Llinas, J., Reiling, V., Sélo, J., 2003. Fluid dynamic numerical simulation of a gas phase polymerization reactor. Int. J. Numer. Methods Fluids 43, 1199–1220.

Hofbauer, H., Rauch, R., Loeffler, G., Kaiser, S., Fercher, E., Tremmel, H., 2002. Six years experience with the FICFB-Gasification Process. In: 12th European Conference and Technology Exhibition on Biomass for Energy, Industry and Climate Protection.

Kunii, D., Levenspiel, O., 1991. Fluidization Engineering. Butterworth Heinemann.

Liu, S.-S., Xiao, W.-D., 2014. Numerical simulations of particle growth in a silicon-CVD fluidized bed reactor via a CFD-PBM coupled model. Chem. Eng. Sci. 111, 112–125.

Liu, M., Wen, Y., Liu, R., Liu, B., Shao, Y., 2015a. Investigation of fluidization behavior of high density particle in spouted bed using CFD-DEM coupling method. Powder Technol. 280, 72–82.

Liu, X., Zhu, C., Geng, S., Yao, M., Zhan, J., Xu, G., 2015b. Two-fluid modeling of Geldart A particles in gas–solid micro-fluidized beds. Particuology 21, 118–127.

Lun, C., Savage, S., 1986. The effects of an impact velocity dependant developed by sheared granular material. Acta Mech. 63, 15–44.

Méchitoua, N., Boucker, M., Laviéville, J., Hérard, J., Pigny, S., Serre, G., 2003. An unstructured finite volume solver for two-phase water/vapour flows modelling based on elliptic oriented fractional step method. In: NURETH 10, Seoul, South Korea.

Mazaudier, F., Proye, C., Hodaj, F., 2008. Further insight into mechanisms of solid-state interactions in UMo/Al system. J. Nucl. Mater. 377 (3), 476–485.

Morioka, S., Nakajima, T., 1987. Modeling of gas and solid particles two-phase flow and application to fluidized bed. J. Theor. Appl. Mech. 6 (1), 77–88.

Neau, H., Laviéville, J., Simonin, O., 2010. NEPTUNE_CFD high parallel computing performances for particle-laden reactive flows. In: 7th International Conference on Multiphase Flow, ICMF 2010, Tampa, FL, May 30–June 4.

Neau, H., Fede, P., Laviéville, J., Simonin, O., 2013. High performance computing (HPC) for the fluidization of particle-laden reactive flows. In: The 14th International Conference on Fluidization, From Fundamentals to Products, Noordwijkerhout, Netherlands.

Pannala, S., Daw, C.S., Finney, C.E., Boyalakuntla, D., Syamlal, M., O'Brien, T.J., 2007. Simulating the dynamics of spouted-bed nuclear fuel coaters. Chem. Vapor Depos. 13 (9), 481–490.

Simonin, O., Février, P., Laviéville, J., 2002. On the spatial distribution of heavy-particle velocities in turbulent flow: from continuous field to particulate chaos. J. Turbul. 3 (1), 1–40.

Srivastava, A., Sundaresan, S., 2003. Analysis of a frictional kinetic model for gas/particle flows. Powder Technol. 129, 72–85.

Thonglimp, V., Hiquily, N., Laguerie, C., 1984. Vitesse minimale de fluidisation et expansion des couches fluidisées par un gaz. Powder Technol. 38, 233–253.

Vahlas, C., Caussat, B., Serp, P., Angelopoulos, G.N., 2006. Principles and applications of CVD powder technology. Mater. Sci. Eng. R: Rep. 53 (1), 1–72.

Vanni, F., Caussat, B., Ablitzer, C., Iltis, X., Bothier, M., 2015a. Silicon coating on very dense tungsten particles by fluidized bed CVD for nuclear application. Phys. Status Solidi (A) 212 (7), 1599–1606.

Vanni, F., Caussat, B., Ablitzer, C., Brothier, M., 2015b. Effects of reducing the reactor diameter on the fluidization of a very dense powder. Powder Technol. 277, 268–274.

Wang, F., Fan, L.-S., 2011. Gas–solid fluidization in mini-and micro-channels. Ind. Eng. Chem. Res. 50 (8), 4741–4751.

Wang, J., Tan, L., Van der Hoef, M., van Sint Annaland, M., Kuipers, J., 2011. From bubbling to turbulent fluidization: advanced onset of regime transition in micro-fluidized beds. Chem. Eng. Sci. 66 (9), 2001–2007.

Wen, C., Yu, Y., 1965. Mechanics of fluidization. Chem. Eng. Symp. Ser. 62, 100–111.

Werther, J., Molerus, O., 1973. The local structure of gas fluidized beds—II. The spatial distribution of bubbles. Int. J. Multiph. Flow 1 (1), 123–138.

Yang, W.-C., 2007. Modification and re-interpretation of Geldart's classification of powders. Powder Technol. 171 (2), 69–74.

Ydstie, B.E., Du, J., 2011. Producing Poly-Silicon from Silane in a Fluidized Bed Reactor. INTECH Open Access Publisher.
Zivkovic, V., Biggs, M., 2015. On importance of surface forces in a microfluidic fluidized bed. Chem. Eng. Sci. 126, 143–149.
Zweifel, T., Palancher, H., Leenaers, A., Bonnin, A., Honkimaki, V., Tucoulou, R., Van Den Berghe, S., Jungwirth, R., Charollais, F., Petry, W., 2013. Crystallographic study of Si and ZrN coated U–Mo atomised particles and of their interaction with al under thermal annealing. J. Nucl. Mater. 442 (1), 124–132.